Magnetically Actuated Protease Sensors for in Vivo Tumor Profiling

Simone Schuerle,[†,§] Jaideep S. Dudani,[†,‡] Michael G. Christiansen,[‖] Polina Anikeeva,[*,‖] and Sangeeta N. Bhatia[*,§,⊥,#,∇,○,◆,¶]

[†]Koch Institute for Integrative Cancer Research, [‡]Department of Biological Engineering, [§]Institute for Medical Engineering and Science, [‖]Department of Materials Science and Engineering, [⊥]Research Laboratory of Electronics, [#]Electrical Engineering and Computer Science, and [∇]Marble Center for Cancer Nanomedicine, Massachusetts Institute of Technology, Cambridge, Massachusetts 02139, United States

[○]Department of Medicine, Brigham and Women's Hospital and Harvard Medical School, Boston, Massachusetts 02115, United States

[◆]Broad Institute of Massachusetts Institute of Technology and Harvard, Cambridge, Massachusetts 02139, United States

[¶]Howard Hughes Medical Institute, Cambridge, Massachusetts 02139, United States

S *Supporting Information*

ABSTRACT: Targeted cancer therapies require a precise determination of the underlying biological processes driving tumorigenesis within the complex tumor microenvironment. Therefore, new diagnostic tools that capture the molecular activity at the disease site in vivo are needed to better understand tumor behavior and ultimately maximize therapeutic responses. Matrix metalloproteinases (MMPs) drive multiple aspects of tumorigenesis, and their activity can be monitored using engineered peptide substrates as protease-specific probes. To identify tumor specific activity profiles, local sampling of the tumor microenvironment is necessary, such as through remote control of probes, which are only activated at the tumor site. Alternating magnetic fields (AMFs) provide an attractive option to remotely apply local triggering signals because they penetrate deep into the body and are not likely to interfere with biological processes due to the weak magnetic properties of tissue. Here, we report the design and evaluation of a protease-activity nanosensor that can be remotely activated at the site of disease via an AMF at 515 kHz and 15 kA/m. Our nanosensor was composed of thermosensitive liposomes containing functionalized protease substrates that were unveiled at the target site by remotely triggered heat dissipation of coencapsulated magnetic nanoparticles (MNPs). This nanosensor was combined with a unique detection assay to quantify the amount of cleaved substrates in the urine. We applied this spatiotemporally controlled system to determine tumor protease activity in vivo and identified differences in substrate cleavage profiles between two mouse models of human colorectal cancer.

KEYWORDS: *Thermoliposomes, proteases, activity-based biomarkers, nanosensors, magnetic nanoparticles, hysteresis-loss heating*
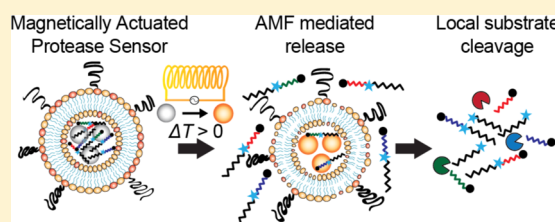
With the advent of targeted therapies, an increasing emphasis has been placed on establishing a system of precision medicine, such that therapies are individually tailored.[1] Robust companion diagnostics are needed to stratify patient disease state and thus inform therapeutic decisions.[1−3] For example, molecular imaging can be used to identify a patient's vascular permeability to nanotherapeutics.[1,4,5] Alternatively, analysis of samples acquired by invasive biopsies can be performed to identify therapeutic regimens (e.g., by analyzing receptor expression). An emerging area of targeted therapies is the application of protease-activated agents, as proteases are known to play role in almost every hallmark of cancer.[6−9] These enzyme-dependent tools are responsive to the local microenvironment, which can improve the therapeutic windows of numerous agents. Protease-activated antibodies, "probodies", being developed are one such example.[10] For the harnessing of the full potential of enzyme-activated interventions, functional diagnostics that provide information on the activity and function of particular proteases within the disease environment are necessary.[1]

Protease activity is typically measured by the cleavage of selective functionalized peptide substrates, which results in contrast generation for imaging purposes.[11−14] We have previously developed multiplexed nanosensors called "synthetic biomarkers" that generate detection signals after proteolytic cleavage of peptide substrates.[15−17] Unlike in situ imaging sensors, the cleavage fragment enters circulation, is concentrated in the urine, and can be detected by a range of analytical techniques (e.g., mass spectrometry or ELISA) enabling noninvasive measurement of in vivo protease activity. However, like other protease sensors, proteolytic cleavage that occurs in circulation or off-target organs affects the specificity of
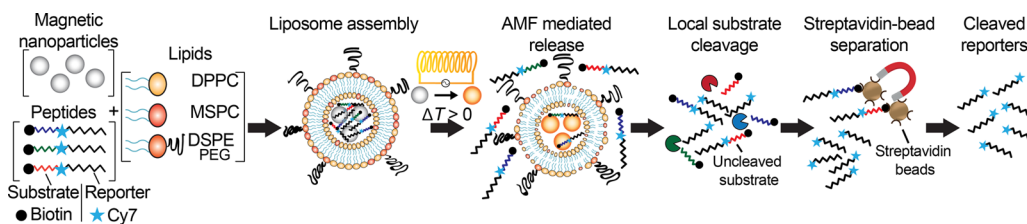
Figure 1. Magnetically actuated protease sensors. Thermosensitive liposomes, consisting of the lipids DPPC, MSPC, and DPSE-PEG, were encapsulated with magnetic nanoparticles and synthetic peptides. These peptide substrates are each coupled with a near-IR dye, Cy7, as a urinary reporter, and an N-terminal biotin enabling streptavidin-bead-based separation. Upon exposure to alternating magnetic fields (AMF), heat is dissipated by the coentrapped MNPs due to hysteresis losses, which in turn melts the thermosensitive bilayer. The permeabilized membrane allows peptides to diffuse to the exterior, where they are cleaved by proteases. Cleaved and uncleaved peptides clear into urine, where cleaved reporters are isolated using streptavidin-coated beads.
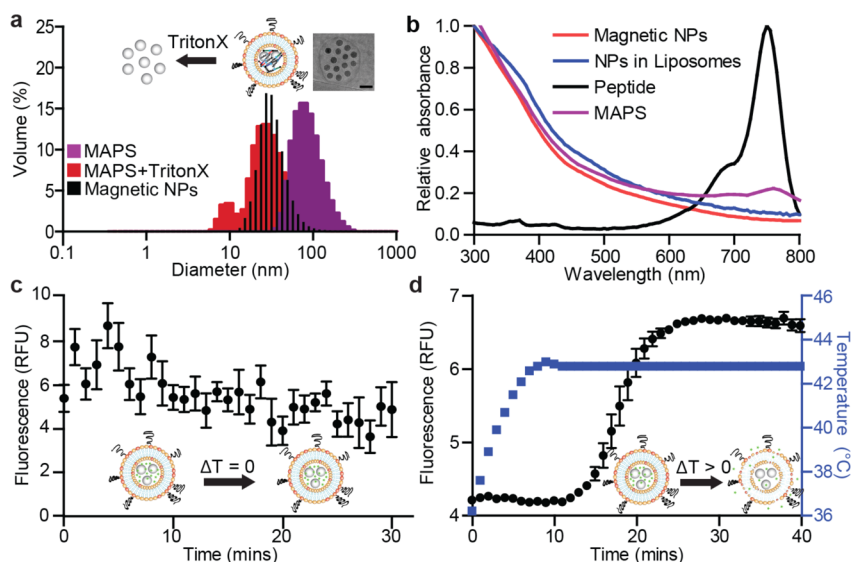

Figure 2. MAPS characterization: size, composition, magnetic properties, and stability. (a) Dynamic light scattering measurements of MAPS (purple) and disrupted MAPS after addition of 0.1% TritonX, showing the release of coentrapped MNPs (red) ($n = 3$). DLS measurement of pure MNPs is overlaid in black. Inset: transmission electron microscopy image of an individual MAPS (scale bar: 50 nm). (b) Absorbance spectra of various components of MAPS. (c) Calcein fluorescence release assay at 37 °C over 30 min ($n = 5$; SEM). (d) At higher temperatures, the release of calcein was detected by increases in sample fluorescence ($n = 5$; SEM).

signal.[18,19] To reduce off-target activation, we recently developed photoactivatable synthetic biomarkers that incorporate photolabile groups to shield access to the peptide substrates and which can reduce the degree of nonspecific signal generation.[20] This technique, however, is challenging to utilize in vivo due to poor penetration of light into most biological tissues.

Here, we report the development of magnetically actuated protease sensors (MAPS) that rely on exposure to local alternating magnetic fields (AMFs) to release peptide substrates from thermosensitive liposomes into the tumor microenvironment, after which they sample and respond to protease activity. In the MAPS platform, peptide substrates are coencapsulated in thermosensitive liposomes with magnetic nanoparticles (MNPs), which undergo hysteretic heat dissipation in the presence of AMFs, leading to elevated local temperatures and liposome deformation. We characterize temperature sensitivity of MAPS and responsiveness to AMFs in vitro and then demonstrate that this newly formulated sensor can distinguish different tumor types by profiling protease cleavage specificities across two xenograft mouse models of colorectal cancer.

Matrix metalloproteinases (MMPs) are a family of structurally related, zinc-dependent endopeptidases with important roles in development, tissue injury and repair, and many diseases.[21,22] In cancer, MMPs promote invasion and metastasis, and different tumors often exhibit unique MMP expression profiles.[22] Thus, we designed a remotely controllable nanosensor to locally assay MMP profiles in tumors.

We employed liposomal carriers to entrap peptide substrates and shield them from nonspecific cleavage in the bloodstream and took advantage of the enhanced permeability and retention (EPR) effect to achieve accumulation at tumor sites.[23,24] To enable thermally induced release of protease-cleavable substrates linked to urinary reporters,[15] liposomes composed of thermosensitive bilayers were coloaded with MNPs that undergo hysteresis and dissipate heat in the presence of AMFs with frequencies in the range of hundreds of kilohertz (Figure 1).

We chose a clinically approved thermosensitive liposome formulation containing DCCP (1,2-dipalmitoyl-*sn*-glycero-3-phosphocholine), which is the most common phosphoglyceride used as a backbone in liposomal bilayer preparations; the lysolipid (MSPC, 1-myristoyl-2-stearoyl-*sn*-glycero-3-phosphocholine); and DSPE-PEG(2000) (1,2-distearoyl-*sn*-phosphoetha-nolamine-N-[amino(polyethylene glycol)-2000]).[25] At the phase-transition temperature, liposomal

bilayers exhibit leaky interfacial regions between the solid and melting liquid phases. For our chosen volume ratio of 80:15:5 for DCCP−MSPC−DSPE-PEG, the critical melting temperature was determined as $T_m \approx 41$ °C,[26,27] and thus, the disruption of our liposomes should require only mild temperature elevation through externally triggered hysteretic heat dissipation.

To achieve the required temperature increase, we chose iron oxide nanoparticles with a diameter of 25 nm (Ocean Nanotech LLC, SHA-25, Figure 2a). The fully assembled MAPS containing MNPs and peptides exhibited a mean diameter of 100 nm, determined on the basis of dynamic light scattering (DLS) measurements (Figure 2a). Successful loading of individual components, i.e. substrates with reporter dye and MNPs, was confirmed by absorbance spectroscopy after filtration (Figure 2b). To quantify MNP loading within the MAPS, iron content was assayed by inductively coupled plasma atomic emission spectrometry (ICP-AES) and found to be 1.89 ± 0.15 mg/mL (Figure S1). Further morphological analysis by transmission electron microscopy (TEM) supported these findings, as MNPs were predominantly entrapped, with only few free MNPs observed (see the inset of Figure 2a and Figure S2).

Prior to applying MAPS to profile MMP activity, we sought to characterize their thermosensitivity and temperature-dependent release profile using a calcein-based assay. Calcein is a membrane impermeable dye that exhibits homoquenching at high concentrations; thus, any release of MAPS-loaded calcein will result in a fluorescence increase. We first probed for any change in permeability at 37 °C and found the liposomes to be stable at this temperature, as the fluorescent signal did not increase (Figure 2c). A substantial release of fluorescence was detected, however, when the temperature of the loaded MAPS samples was raised to 43 °C (Figure 2d). Both the steep slope and magnitude of the response are indicative of a robust and sensitive change in liposome permeability.

Next, we determined the AMF parameters necessary for sufficient hysteretic heating rates (specific loss power, SLP) in entrapped MNPs to induce magnetothermal melting of the liposomal bilayer. SLP depends on the amplitude and frequency of the externally applied AMF as well as MNP properties, such as size, shape, and composition.[28] For a MNP solution, the SLP is calculated as $SLP = \frac{C}{m} \times \frac{\Delta T}{\Delta t}$, where C is the specific heat capacity of water ($C = 4.184$ J K^{-1} mL^{-1}), m is the iron concentration (in g$_{(Fe)}$/mL), and $\Delta T/\Delta t$ is the experimentally measured initial slope of the temperature increase under AMF exposure.

Although previous studies have reported liposomes loaded with small iron oxide MNPs in the size range of 5−15 nm,[23] we instead chose comparatively larger 25 nm MNPs due to their higher SLP. This selection is motivated by dynamic hysteresis modeling,[29,30] combined with a limit on permissible amplitude-frequency products for continuous exposure ($H_o \times f \approx 5 \times 10^9$ A·m^{-1}·s^{-1}).[31] We have previously suggested that maximized heating rates subject to this constraint are achieved by using particles with relaxation times exceeding the time scale set by the AMF frequency at field magnitudes close to their effective anisotropy field. Additionally, this previous work identified that spherical iron oxide particles with 25 nm diameters exhibit high SLPs, and high individual particle loss powers (IPLPs), at AMF conditions similar to those employed here.[29] A detailed analysis of IPLPs for different particle sizes that motivated our particle

choice has been published recently.[32] Based on calorimetry measurements, an AMF signal with an amplitude of 15kA/m and frequency of 515 kHz was found to produce an SLP of 610 ± 16 W/g$_{(Fe)}$ (Figure 3a and inset). Recent studies have
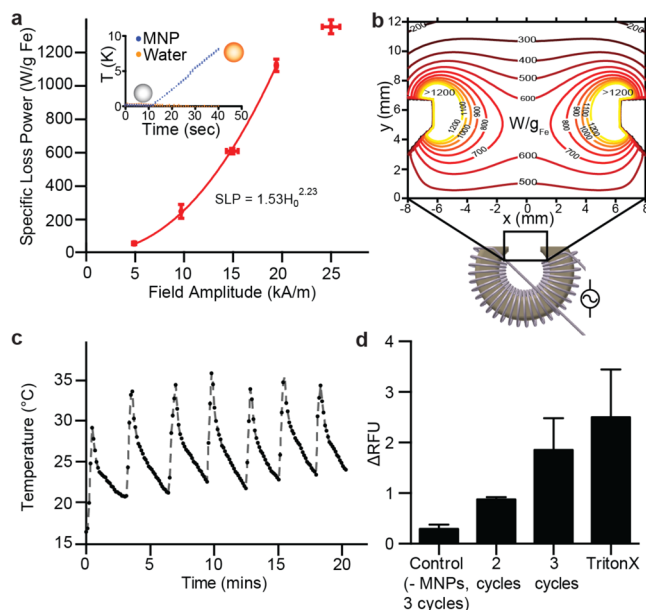

Figure 3. Magnetothermal activation: coil design and parameter determination for magnetically induced release. (a) Optimal AMF parameters were evaluated by calorimetric measurements. Fit line interpolated using a power law valid for field strength magnitudes between 0 and 20 kA/m ($n = 3$; SEM). Inset: fluid temperature increase during 30 s of AMF exposure at 515 kHz and 15 kA/m ($n = 5$). (b) Technical drawing of coil with ferromagnetic core utilized in studies. Inset shows the distribution of the specific loss power (SLP) for 25 nm particles at 515 kHz across the 12.5 mm wide gap. SLP values were derived on the basis of the interpolation of the measurements shown in (a) at 515 kHz and varying field amplitude. (c) Infrared thermal camera measurements of heat dissipation in the coil gap during a duty cycle of 40 s on time and 240 s off. (d) Liposomes prepared with quenched calcein solution and with and without MNPs were exposed to an AMF sequence (515 kHz, 15 kA/m for 40 s). Fluorescence release was quantified. The release profiles were compared to fluorescence signal increase by the addition of TritonX, which destroys the liposomal structure ($n \geq 2$; SEM).

reported a large temperature increase near the surface of nanoparticles,[33,34] and such local heating may play a mechanistic role in release.[32] We were further interested in potential particle−particle interactions, given the local MNP accumulation in liposomes that could influence the magnetic response.[35] Analysis by vibrating sample magnetometry revealed superparamagnetic behavior with convergence to nearly the same slope in the limit of a low applied field for both the pure MNPs and suspensions of liposomes with encapsulated MNPs (Figure S3). However, the encapsulated MNPs approach saturation more gradually than the free particles. Both of these qualitative features are predicted for noninteracting ensembles of randomly oriented particles with increasing anisotropy.[30]

To produce the AMF conditions identified above in up to 1 cm large tumors, we designed a coil consisting of litz wire wound around a soft ferromagnetic toroid core with a 12.5 mm gap (Figures 3b and S4) that delivers the necessary stimulus without significant overheating (Figures 3c and S5). We

determined a duty cycle consisting of 40 s AMF exposures separated by 240 s rest, which permitted steady-state operation (Figure S5). Modeling of the expected field amplitude profile was used in combination with interpolated calorimetry data to predict how SLP would vary with position across the exposed tumor volume (Figure 3b).

To quantify the release dynamics, we exposed samples with and without MNPs to AMF pulses and measured relative fluorescence using the calcein release assay described above. The fluid temperature was monitored with a fiber optic thermometer, ensuring that stray heat from the setup did not exceed 38 °C. Exposing liposomes containing MNPs to an increasing number of AMF cycles led to a corresponding increase in fluorescence (Figure 3d). The relative fluorescence signal did not increase significantly when control samples, which did not contain MNPs, were tested (Figure 3d). Liposome disruption using the detergent Triton X-100 resulted in fluorescence increase on par with AMF-triggered release (Figure 3d).

For the purpose of loading the liposomes with candidate tumor responsive protease substrates, we chose three peptide substrates that respond to MMPs on the basis of our previous work.[15] These protease substrates are each linked to a D stereoisomer of glutamate fibrinopeptide coupled with a near-infrared (IR) dye, Cy7, as a urinary reporter, similar to our previous synthetic biomarker constructs (Figure 4a and Table S1). In contrast to our earlier approaches, the peptide-reporter conjugates used here for liposome loading are not tethered directly to nanoparticle surfaces. Because kidney filtration is efficient for molecules less than 5 nm in size, unconjugated peptides could filter through to the urine even in the absence of

proteolysis.[36] To circumvent this source of false positive signals, we developed an assay to deplete uncleaved substrates. We coupled biotin to the N-terminus of all peptides, which can be efficiently captured using streptavidin beads. Uncleaved substrates will retain the N-terminal biotin and thus be efficiently eliminated (Figure S6a). We validated this detection method by first confirming the ability to completely remove excess uncleaved substrate by measuring the fluorescence signal of free peptide sequences in phosphate buffered saline (PBS) and 2% urine, before and after streptavidin bead separation (Figure S6b,c). Cy7 measurements were robust and could be measured over several log dilutions using an IR fluorescence scanner (Figure S7). Moreover, we confirmed the shielding mechanism of the liposomal bilayer by incubating MAPS with streptavidin beads and subsequently exposing the sample to a permanent magnet (Figure S8). Using this new detection method, we measured relative proteolysis of the substrates by several MMPs (Figure 4b,c). With hierarchical clustering, S1 and S3 performed similarly and responded primarily to MMP2 and MMP9. S2 was cleaved efficiently by MMP7 and MMP19 (Figure 4c).

With all of the components of our MAPS platform validated in vitro, we next sought to assay the performance of our magnetically actuated, thermosensitive particles bearing MMP substrate reporters in vivo. As a first step, we determined the blood half-life of fluorescently labeled liposomes in healthy Swiss Webster mice to be approximately 1 h, which we hypothesized to be sufficient to allow for passive accumulation at the tumor (Figure S9a). To identify the optimal time point for remote AMF triggering of reporter release from nano-sensors, we measured accumulation of liposomes in organs and in tumor xenografts of the human colon cancer cell line LS174T, which has been used extensively for in vivo cancer models and secretes active MMPs, including MMP2 and 9 (Figure S9b).[37] We determined that the optimal time for tumor activation of the MAPS was 3 h post-administration, as there should be relatively low blood concentration (due to a half-life of approximately 1 h) and reasonable tumor accumulation for specific activation.

We applied MAPS to profile tumor protease activity in vivo. To assay for the specific release of MAPS-delivered reporters, we first intravenously injected MAPS-S3 in two cohorts of LS174T flank-tumor-bearing mice. For the establishment of a baseline signal and thus control for any nonspecific liposome release and background noise, urine from both cohorts was collected 1 h after MAPS administration. A total of 2 h later, mice from one group were exposed to AMF by positioning the flank tumor within the 12.5 mm gap present in the custom-made AMF coil, and a second urine collection was performed 1 h after the AMF treatment (Figures 5a and S10). As expected, at the 1 h time point, prior to AMF exposure, all mice displayed uniform, urine reporter fluorescence (Figure 5b), likely a result of nonspecific leakage from the liposomes and subsequent proteolytic cleavage. In contrast, following the application of two AMF pulses to the tumor site, a statistically significant fluorescence increase was observed in the urine samples, only for the activated group (Figure 5c). This outcome demonstrates the proof-of-principle, heat-dependent local release of labeled peptide substrates from MAPS, exposing them to proteolytic cleavage.

Having established that our MAPS constructs are sensitive to targeted release via AMF administration, we next aimed to test whether our MAPS (S1−S3) could be used to distinguish
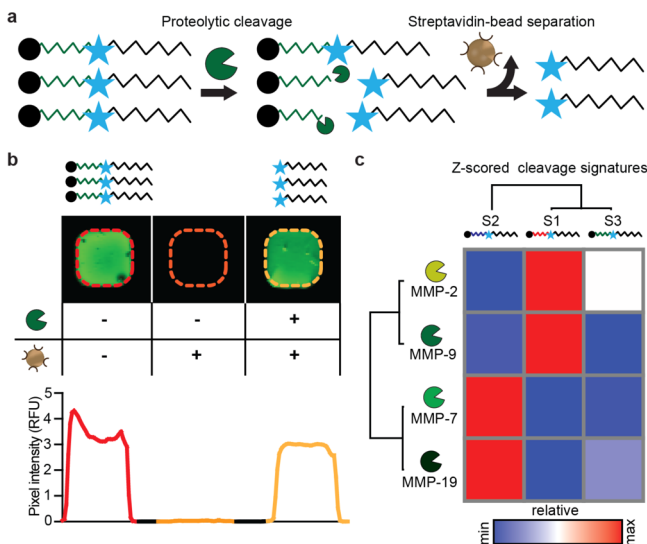

Figure 4. Characterization of cleavage quantification assay and protease specificities. (a) Schematic of assay. The N-terminal biotin identifies an uncleaved substrate, which can be depleted using streptavidin beads. Measurements of cleaved reporters are enabled by a Cy7 fluorophore. (b) Left: Cy7 signal of an initial peptide solution. Middle: no fluorescence signal was detected after depletion of uncleaved substrates with streptavidin beads Right: addition of MMP9 and subsequent streptavidin depletion results in similar fluorescent levels as the initial peptide solution, showing robust cleavage of the substrate. (c) Recombination assay was performed for three distinct peptides substrates. Data were clustered via hierarchical clustering (one minus Pearson correlation), revealing substrate cleavage patterns.
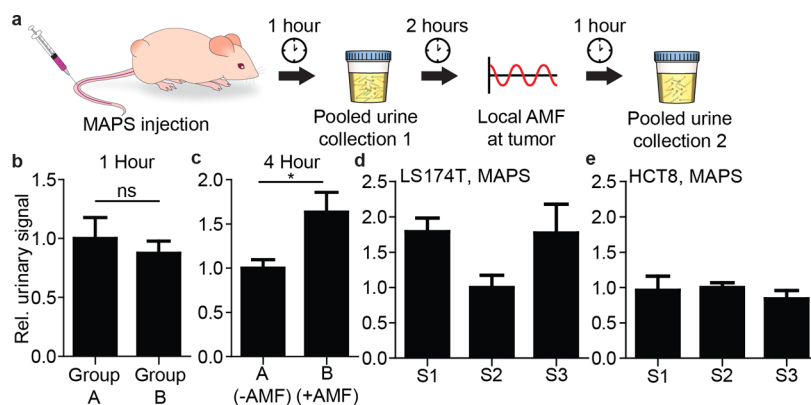
Figure 5. MAPS enabling of in vivo profiling of protease activity in tumors. (a) Schematic of the in vivo profiling assay. A total of 1 h after MAPS administration, urine was collected to measure background signal. A total of 3 h post-injection, AMF was applied locally at the tumor to one group and urine collected 1 h after activation. (b) Prior to activation, two cohorts of mice show similar urine reporter concentrations. (c) After activation, significantly greater urine reporter concentrations can be detected in the group exposed to AMF ($n = 5$; *, $P < 0.05$ Student's t test; data normalized to Group A). MAPS urinary signatures after activation across the three substrates for (d) LS174T and (e) HCT-8 reveal that S1 and S3 are cleaved at greater rate relative to S2 in LS174T tumors ($n \geq 5$ per group; data normalized to S2 signal for both LS174T and HCT8).

between distinct tumor-derived cell-lines, due to differences in their in vivo MMP profiles. The ability to classify clinical tumors on the basis of MMP profiles would provide valuable input during therapy selection. For comparison, we chose another human colon carcinoma line, HCT-8, which has been validated previously to secrete lower levels of MMP9 than LS174T in vitro.[19] Additionally, we measured MMP2 levels in cell culture supernatant by ELISA and found that HCT-8 cells secrete lower amounts of MMP2 compared to LS174T (Figure S11a). We tested for cleavage of our substrates by cell-secreted proteases by employing fluorescently quenched versions and exposing them to conditioned supernatant. From these in vitro cleavage assays, S1 was cleaved most significantly by LS174T proteases, whereas minimal cleavage of S2 and S3 was observed (Figure S11b). In vitro proteolysis was abrogated in the presence of Marimastat, an MMP inhibitor. In contrast, none of the substrates were efficiently cleaved by HCT-8 secreted proteases (Figure S11c).

After the in vitro optimization steps, we generated flank tumors using the two cell lines. Following administration of the pooled sets of MAPS particles, we applied the in vivo activation protocol and collected urine in an effort to detect distinct profiles of protease activity between LS174T and HCT8 tumors. Indeed, in response to the localized, in vivo activation of our magnetothermally triggered nanosensors, we measured elevations in both MAPS-S1 and MAPS-S3 urinary signals, relative to the levels of the MAPS-S2 cleaved substrates in LS174T tumor-bearing mice (Figure 5d). In contrast, all three constructs generated similar urine signals with respect to each other when tested in mice with HCT8-derived tumors (Figure 5e), which is consistent with the relatively low MMP2 and 9 secretion rates, as S1 and S3 respond strongly to MMP2 and 9 (Figure 4c). This differing pattern of substrate release highlights that MAPS have the capacity to distinguish the protease activities present in the tumors derived from two different colon cancer types. Injection of free peptide into healthy mice showed that S3 had the lowest background cleavage, validating its previous application as a robust substrate for profiling protease activity of cancers with high sensitivity and specificity (Figure S12a).[17] In contrast to the MAPS signature of LS174T flank tumor-bearing mice, injection of free peptides (i.e., unencapsulated in liposomes) into these mice, which should

primarily sample blood activity (including proteases secreted from the tumor into the blood),[19] showed similar S2 and S3 signals and an elevated S1 signal (Figure S12b). Taken together, these results emphasize the importance of shielding protease access to circulating, activity-based reporters when seeking to sample local protease activities and highlight the capability of MAPS to distinguish in vivo protease profiles of two human colon cancer lines with differing protease levels (Figure S11 and S12).

In summary, we report an approach to measure tumor protease activity in vivo with greater specificity using remotely addressable nanosensors. We demonstrate that peptides are shielded in our thermosensitive MNP-containing liposomes and can be locally released in the tumor microenvironment via external application of AMFs. This system is not hindered by optical windows and allows for deep-tissue activation. We demonstrate that this technique is able to identify differences in MMP profiles across two in vivo human colorectal cancer xenograft models. The urinary reporters employed can be readily multiplexed (e.g., by mass encoding[15]) to enable high-content profiling of tumors. Furthermore, multimodal diagnosis and profiling could be enabled by magnetic resonance imaging for the magnetic nanoparticles within the liposomes. We primarily apply MAPS to profile MMP activity, but this approach is readily applicable to a variety of enzyme families. MAPS will prove valuable in the development, validation, and application of protease-targeted therapeutics.

Materials and Methods. *Synthesis of Peptide Substrates and Liposomes.* Peptides were synthesized by CPC Scientific, Inc. For the full peptide sequence and description, see the Supporting Information. Briefly, peptide-reporter tandems are composed of an N-terminal biotin for depletion, followed by protease substrate, and then the D stereoisomer of glutamate fibrinopeptide conjugated to Cy7 for urinary measurements. Liposomes were prepared by applying the lipid-film hydration method with subsequent sequential extrusion. A lipid composition of 11.18 mg of dipalmitoylphosphatidyl-choline, 1.31 mg of monostearoylphosphatidylcholine, and 2.51 mg of poly(ethylene glycol)-conjugated distearoylphosphatidyletha-nolamine was dissolved in 1.5 mL of isopropanol and shortly sonicated, and three aliquots of each (0.5 mL) were dried under gentle nitrogen flow. All components were purchased from

Avanti Polar lipids. The formed lipid cakes were then kept at least for 12 h under vacuum. A volume of 300 μL of Trizma-based hydration media was prepared and mixed with magnetic nanoparticles (Ocean Nanotech, SHA-25) at a final iron concentration of 2.5 mg/mL and DMSO-based peptide solutions at a concentration of 2 μM. The solution was prewarmed to 65 °C and added to the liposomal cake, which was hydrated for 1 h at 65 °C in a water bath under continuous agitation. For in vitro release studies, 80 mM calcein was added to the Trizma solution instead of peptide substrates. At this concentration, the self-quenching properties of calcein in solution were ensured. After hydration, the liposomes were extruded sequentially using 400, 200, and 100 nm large filter membranes to narrow the size distribution. The solutions were then purified from excess particles and free substrates by gravity column filtration. The resulting size was quantified by dynamic light scattering, and peptide and iron concentration were measured by absorbance scans. The final solutions for in vivo injection were equally adjusted to 0.5 μM for peptides S1, S2, and S3 by dilution in PBS.

In Vitro Thermorelease Studies. Temperature stability and kinetic release profile were measured in a fluorescence plate reader (Tecan) by suspending MAPS samples of 80 μL in 384 well plates. Temperature was set and kept at 37 °C and increased to 43 °C for kinetic release measurements when crossing the melting temperature. Calcein release was determined by measuring the increase of the fluorescence signal for an excitation wavelength of λ_{ex}= 494 nm and an emission wavelength of λ_{em}= 517 nm.

Magnetic Activation of Thermosensitive Liposomes. Magnetic activation of the liposomes was performed using a custom AMF setup. A pair of coils were fabricated and specifically designed to fit the requirements for in vitro and in vivo experiments. A toroid composed of a soft ferromagnetic material optimized for high-frequency power transformers (Ferroxcube 3F3) was used as the coil core. A transformer circuit with a resistive ballast in the primary circuit was used to generate high, stable currents in the secondary while simultaneously matching the impedance of the variable frequency 200 W amplifier (1020L, Electronics & Innovation). In the secondary, the coil acted as the resistive and inductive elements of an RLC resonance circuit, with a high-voltage series capacitor setting the resonant frequency. The field magnitude was measured by a custom built probe employing a pickup loop and an oscilloscope. A simple cooling system with circulating ice water was coupled to the coil via silicone tubing, and an electric fan was positioned in proximity to the coil. For in vitro release studies and calorimetric measurements of the particles, temperature measurements were conducted using an AMF insensitive fiber optic temperature probe and recorded during AMF exposure. SLP measurements were repeated three times, and control samples with only water were measured after every four trials to determine the background heating rate. All samples were 0.1 mL, with a MNP concentration of approximately 2 mg/mL. The SLP value measured was normalized to the metal content determined by elemental analysis. In vitro release studies were temperature-monitored, and fluid temperatures did not exceed T = 39 °C due to background heating. Measurements were repeated three times, and calcein release was evaluated in a multiwell plate fluorescence reader as described above.

In Vitro Recombinant Protease Assays. MMPs (∼100 nM working concentration, Enzo Life Sciences) were added to substrates in 384 well plates in activity buffer (50 mM Tris, 150 mM NaCl, 5 mM CaCl2, and 1 μM ZnCl2) containing 1% BSA. After 1 h, uncleaved peptide was extracted using Dynabeads Strepatividin C1 (Life Technologies) as per manufacturer protocols. An excess of Dynabeads was used.

Cell Culture and Secreted Protease Activity Assay. LS174T and HCT-8 cells were cultured in Eagle's Minimal Essential Medium (ATCC) supplemented with 10% FBS (Gibco) and 1% penicillin-streptomycin (CellGro). Cells were passaged when confluence reached 80%. For the isolation of secreted proteases, after cells were plated, cells were washed and replaced in serum-free media. Media was collected and MMP2 was measured in supernatant using a Quantikine MMP-2 kit following manufacturer protocols (R&D Systems). Secretion was normalized to number of cells and days in culture. A similar approach was used when collecting supernatants for measuring the proteolysis of S1–3.

Pharmacokinetic Studies. Wild-type, female Swiss Webster mice (4−6 weeks, Taconic) were infused intravenously via the tail vein with liposomes carrying a near-IR dye (VT750, PerkinElmer). Blood was withdrawn retro-orbitally (∼10 μL) and then immediately transferred into 90 μL of PBS with 5 mM EDTA and spun at 1000g to pellet blood cells. Concentration of liposome was measured using an Odyssey Infrared scanner (Li-Cor Inc.). Nude mice bearing LS174T tumors (see below) were infused with labeled liposomes. Mice were sacrificed at different time points, followed by necropsy to remove organs and tumors. Organ accumulation was measured using an Odyssey scanner and quantified using ImageJ (NIH).

In Vivo Cancer Model Studies. Female nude mice (4−6 weeks, Taconic) were inoculated subcutaneously with 3×10^6 LS174T cells and HCT-8 cells on the hind flank and allowed to grow. A total of 2 weeks after inoculation, tumor-bearing mice were infused with MAPS. Suspensions were diluted to each 0.5 μM peptide concentration in 200 μL of sterile PBS. Immediately after infusion, mice were placed in an in-house devised urine collector with a 96 well plate base. Urine was collected and stored at −80 °C. For analysis, urine was diluted to 25-fold in PBS. Reporter concentration was quantified by Cy7 fluorescence measurements in the Odyssey Scanner and compared to a ladder (Figure 9).

Statistics and Data Analysis. All statistical analyses were performed in GraphPad (Prism 5.0). Statistical significance and individual tests are described in figure legends. Heatmaps and hierarchical clusters were generated using GENE-E (Broad Institute). Data were clustered by one minus Pearson correlation.

■ ASSOCIATED CONTENT

S **Supporting Information**

The Supporting Information is available free of charge on the ACS Publications website at DOI: 10.1021/acs.nano-lett.6b02670.

Figures showing measurements of MAPS solution, cryo-transmission electron micrographs of liposomes with entrapped magnetic nanoparticles, characterization of sample magnetization, simulations of field amplitude for varying gap sizes, IR measurements during operation, urine depletion of uncleaved substrates, Cy7 ladder reading on IR scanner, peptides are shielded inside liposomes, pharmacokinetic characterization of MAPS, IR measurements during in vivo operation, in vitro

cellular protease analysis and comparison, and in vivo performance of unencapsulated S1−3 peptides. A table showing sequences of peptides employed in study. (PDF)

AUTHOR INFORMATION

Corresponding Authors
*P.A. address: Massachusetts Institute of Technology, 77 Massachusetts Avenue, Building 8-425, Cambridge, MA 02139, United States; phone: +1 617-253-3301; e-mail: anikeeva@mit.edu.

*S.N.B. address: Massachusetts Institute of Technology, 77 Massachusetts Avenue, Building 76-453, Cambridge, MA 02139, United States; phone: +1 617 324 0610; e-mail: sbhatia@mit.edu.

Author Contributions
S.S. and J.S.D. contributed equally.

Notes
The authors declare no competing financial interest.

REFERENCES
(1) Friedman, A. A.; Letai, A.; Fisher, D. E.; Flaherty, K. T. *Nat. Rev. Cancer* **2015**, *15* (12), 747−756.

(2) Papadopoulos, N.; Kinzler, K. W.; Vogelstein, B. *Nat. Biotechnol.* **2006**, *24* (8), 985−995.

(3) Hori, S. S.; Gambhir, S. S. *Sci. Transl. Med.* **2011**, *3* (109), 109ra116−109ra116.

(4) Miller, M. A.; Gadde, S.; Pfirschke, C.; Engblom, C.; Sprachman, M. M.; Kohler, R. H.; Yang, K. S.; Laughney, A. M.; Wojtkiewicz, G.; Kamaly, N.; Bhonagiri, S.; Pittet, M. J.; Farokhzad, O. C.; Weissleder, R. *Sci. Transl. Med.* **2015**, *7* (314), 314ra183−314ra183.

(5) Gambhir, S. S. *Nat. Rev. Cancer* **2002**, *2* (9), 683−693.

(6) Hanahan, D.; Weinberg, R. A. *Cell* **2011**, *144* (5), 646−674.

(7) López-Otín, C.; Bond, J. S. *J. Biol. Chem.* **2008**, *283* (45), 30433−30437.

(8) Choi, K. Y.; Swierczewska, M.; Lee, S.; Chen, X. *Theranostics* **2012**, *2* (2), 156−178.

(9) Fortelny, N.; Cox, J. H.; Kappelhoff, R.; Starr, A. E.; Lange, P. F.; Pavlidis, P.; Overall, C. M. *PLoS Biol.* **2014**, *12* (5), e1001869.

(10) Desnoyers, L. R.; Vasiljeva, O.; Richardson, J. H.; Yang, A.; Menendez, E. E. M.; Liang, T. W.; Wong, C.; Bessette, P. H.; Kamath, K.; Moore, S. J.; Sagert, J. G.; Hostetter, D. R.; Han, F.; Gee, J.; Flandez, J.; Markham, K.; Nguyen, M.; Krimm, M.; Wong, K. R.; Liu, S.; Daugherty, P. S.; West, J. W.; Lowman, H. B. *Sci. Transl. Med.* **2013**, *5* (207), 207ra144−207ra144.

(11) Mahmood, U.; Weissleder, R. *Mol. Cancer Ther.* **2003**, *2* (5), 489−496.

(12) Hilderbrand, S. A.; Weissleder, R. *Curr. Opin. Chem. Biol.* **2010**, *14* (1), 71−79.

(13) Whitney, M.; Savariar, E. N.; Friedman, B.; Levin, R. A.; Crisp, J. L.; Glasgow, H. L.; Lefkowitz, R.; Adams, S. R.; Steinbach, P.; Nashi, N.; Nguyen, Q. T.; Tsien, R. Y. *Angew. Chem., Int. Ed.* **2013**, *52* (1), 325−330.

(14) Whitley, M. J.; Cardona, D. M.; Lazarides, A. L.; Spasojevic, I.; Ferrer, J. M.; Cahill, J.; Lee, C.-L.; Snuderl, M.; Blazer, D. G.; Hwang, E. S.; Greenup, R. A.; Mosca, P. J.; Mito, J. K.; Cuneo, K. C.; Larrier, N. A.; O'Reilly, E. K.; Riedel, R. F.; Eward, W. C.; Strasfeld, D. B.; Fukumura, D.; Jain, R. K.; Lee, W. D.; Griffith, L. G.; Bawendi, M. G.; Kirsch, D. G.; Brigman, B. E. *Sci. Transl. Med.* **2016**, *8* (320), 320ra4−320ra4.

(15) Kwong, G. A.; von Maltzahn, G.; Murugappan, G.; Abudayyeh, O.; Mo, S.; Papayannopoulos, I. A.; Sverdlov, D. Y.; Liu, S. B.; Warren, A. D.; Popov, Y.; Schuppan, D.; Bhatia, S. N. *Nat. Biotechnol.* **2013**, *31* (1), 63−70.

(16) Lin, K. Y.; Kwong, G. A.; Warren, A. D.; Wood, D. K.; Bhatia, S. N. *ACS Nano* **2013**, *7*, 9001.

(17) Warren, A. D.; Kwong, G. A.; Wood, D. K.; Lin, K. Y.; Bhatia, S. N. *Proc. Natl. Acad. Sci. U. S. A.* **2014**, *111* (10), 3671−3676.

(18) Miller, M. A.; Barkal, L.; Jeng, K.; Herrlich, A.; Moss, M.; Griffith, L. G.; Lauffenburger, D. A. *Integr. Biol.* **2011**, *3* (4), 422−438.

(19) Kwong, G. A.; Dudani, J. S.; Carrodeguas, E.; Mazumdar, E. V.; Zekavat, S. M.; Bhatia, S. N. *Proc. Natl. Acad. Sci. U. S. A.* **2015**, *112*, 12627−12632.

(20) Dudani, J. S.; Jain, P. K.; Kwong, G. A.; Stevens, K. R.; Bhatia, S. N. *ACS Nano* **2015**, *9* (12), 11708−11717.

(21) Kessenbrock, K.; Plaks, V.; Werb, Z. *Cell* **2010**, *141* (1), 52−67.

(22) Egeblad, M.; Werb, Z. *Nat. Rev. Cancer* **2002**, *2* (3), 161−174.

(23) Torchilin, V. P. *Nat. Rev. Drug Discovery* **2005**, *4* (2), 145−160.

(24) Allen, T. M.; Cullis, P. R. *Adv. Drug Delivery Rev.* **2013**, *65* (1), 36−48.

(25) Needham, D.; Park, J.-Y.; Wright, A. M.; Tong, J. *Faraday Discuss.* **2013**, *161*, 515−534 discussion 563−589..

(26) Li, L.; ten Hagen, T. L. M.; Schipper, D.; Wijnberg, T. M.; van Rhoon, G. C.; Eggermont, A. M. M.; Lindner, L. H.; Koning, G. A. *J. Controlled Release* **2010**, *143* (2), 274−279.

(27) Li, L.; ten Hagen, T. L. M.; Hossann, M.; Süss, R.; van Rhoon, G. C.; Eggermont, A. M. M.; Haemmerich, D.; Koning, G. A. *J. Controlled Release* **2013**, *168* (2), 142−150.

(28) Glöckl, G.; Hergt, R.; Zeisberger, M.; Dutz, S.; Nagel, S.; Weitschies, W. *J. Phys.: Condens. Matter* **2006**, *18* (38), S2935.

(29) Christiansen, M. G.; Senko, A. W.; Chen, R.; Romero, G.; Anikeeva, P. *Appl. Phys. Lett.* **2014**, *104* (21), 213103.

(30) Carrey, J.; Mehdaoui, B.; Respaud, M. *J. Appl. Phys.* **2011**, *109* (8), 083921.

(31) Hergt, R.; Dutz, S. *J. Magn. Magn. Mater.* **2007**, *311* (1), 187−192.

(32) Romero, G.; Christiansen, M. G.; Stocche Barbosa, L.; Garcia, F.; Anikeeva, P. *Adv. Funct. Mater.* **2016**, DOI: 10.1002/adfm.201602189.

(33) Dong, J.; Zink, J. I. *ACS Nano* **2014**, *8* (5), 5199−5207.

(34) Riedinger, A.; Guardia, P.; Curcio, A.; Garcia, M. A.; Cingolani, R.; Manna, L.; Pellegrino, T. *Nano Lett.* **2013**, *13* (6), 2399−2406.

(35) Allia, P.; Tiberto, P.; Coisson, M.; Chiolerio, A.; Celegato, F.; Vinai, F.; Sangermano, M.; Suber, L.; Marchegiani, G. *J. Nanopart. Res.* **2011**, *13* (11), 5615−5626.

(36) Soo Choi, H.; Liu, W.; Misra, P.; Tanaka, E.; Zimmer, J. P.; Itty Ipe, B.; Bawendi, M. G.; Frangioni, J. V. *Nat. Biotechnol.* **2007**, *25* (10), 1165−1170.

(37) Brand, K.; Baker, A. H.; Perez-Cantó, A.; Possling, A.; Sacharjat, M.; Geheeb, M.; Arnold, W. *Cancer Res.* **2000**, *60* (20), 5723−5730.

Supplemental Information

Magnetically actuated protease sensors for *in vivo* tumor profiling

Simone Schuerle[1,3, §], Jaideep S. Dudani[1,2, §], Michael G. Christiansen[4], Polina Anikeeva[4,*], Sangeeta N. Bhatia[3,5-10,*]

1. Koch Institute for Integrative Cancer Research, Massachusetts Institute of Technology, Cambridge, MA 02139
2. Department of Biological Engineering, Massachusetts Institute of Technology, Cambridge, MA 02139
3. Institute for Medical Engineering and Science, Massachusetts Institute of Technology, Cambridge, MA 02139
4. Department of Materials Science and Engineering, Massachusetts Institute of Technology, Cambridge, MA 02139, USA.
5. Research Laboratory of Electronics, Massachusetts Institute of Technology, Cambridge, MA 02139, USA
6. Electrical Engineering and Computer Science, Massachusetts Institute of Technology, Cambridge, MA 02139
7. Marble Center for Cancer Nanomedicine, Massachusetts Institute of Technology, Cambridge, MA 02139
8. Department of Medicine, Brigham and Women's Hospital and Harvard Medical School, Boston, MA 02115
9. Broad Institute of Massachusetts Institute of Technology and Harvard, Cambridge, MA 02139
10. Howard Hughes Medical Institute, Cambridge, MA 02139

§ Equally contributing authors
*Corresponding Authors:

Address: Massachusetts Institute of Technology, 77 Massachusetts Avenue, Building 76-453, Cambridge, MA 02139, USA.
Phone: +1 617 324 0610
Email: sbhatia@mit.edu

Address: Massachusetts Institute of Technology, 77 Massachusetts Avenue, Building 8-425, Cambridge, MA 02139, USA.
Phone: +1 617-253-3301
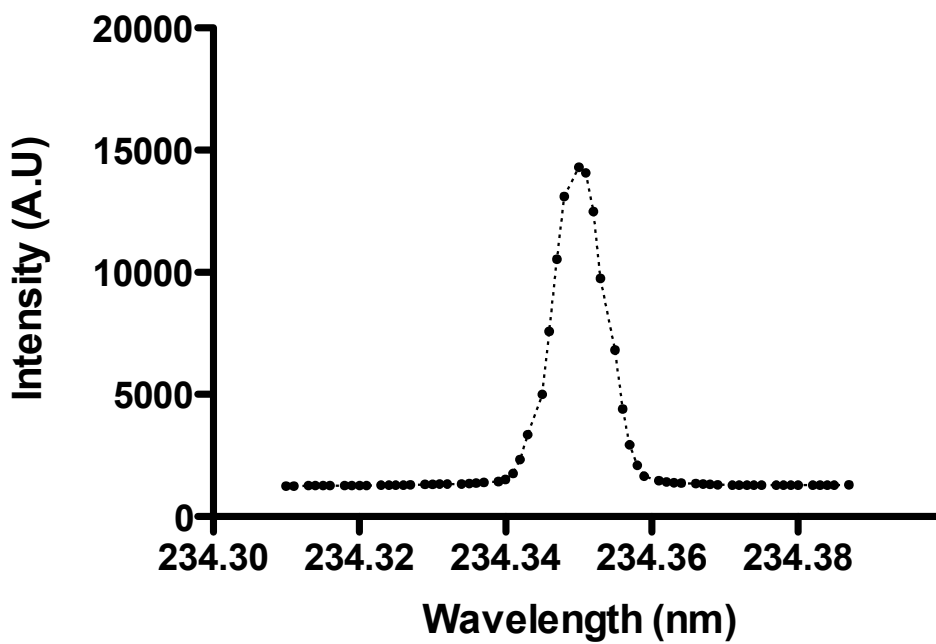Email: anikeeva@mit.edu

Figure S1. ICP-AES. Measurements of MAPS solution showing the peak for the 234.5 nm Fe line. Prior measurements, the samples were digested by heating of the sample for 2 hours at 500 °C to remove organics followed by addition of hydrochloric acid to dissolve the sample and final suspension in 2% nitric acid.
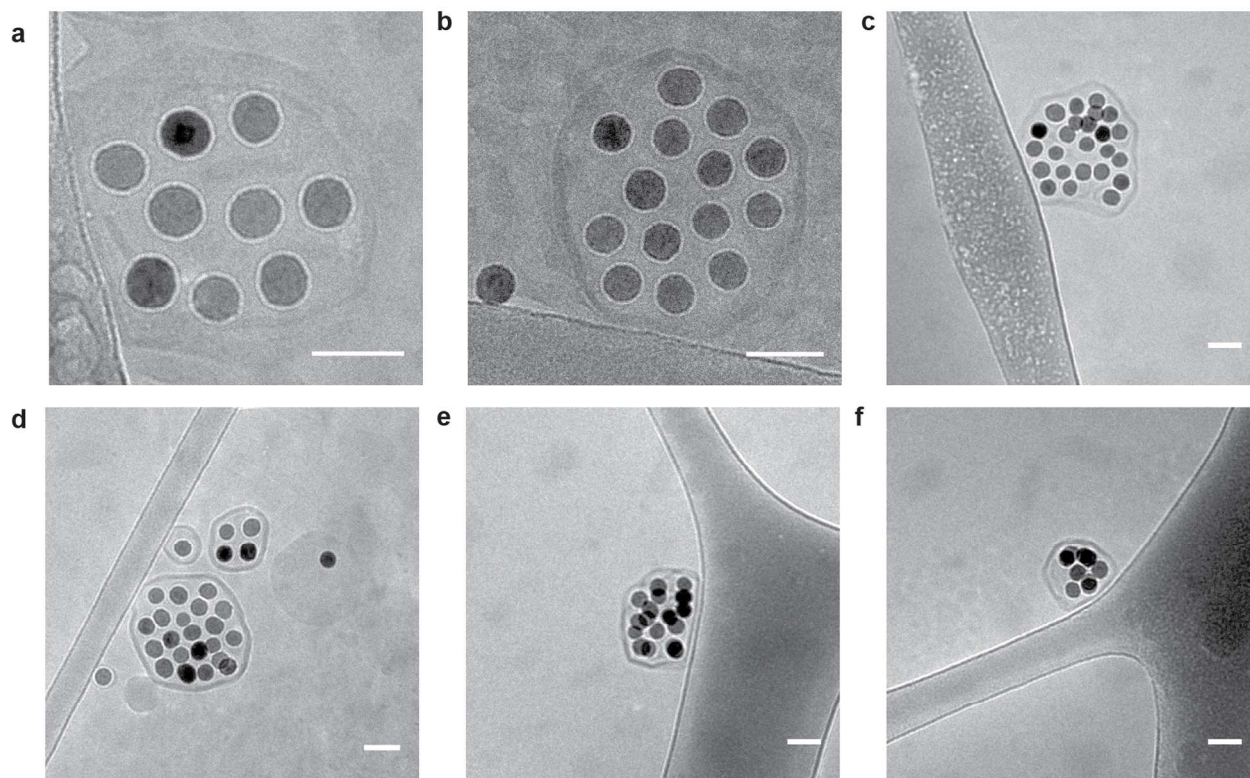
Figure S2. Cryo-Transmission electron micrographs of liposomes with entrapped magnetic nanoparticles. A sample of liposomes with MNPs was prepared for high resolution imaging by cryo-freezing. Despite a few free MNPs, given the high initial loading concentration during liposomal formation, we predominately we found MNPs entrapped inside the liposomal membranes as depicted in (a-f). Scale bars: 50 nm.
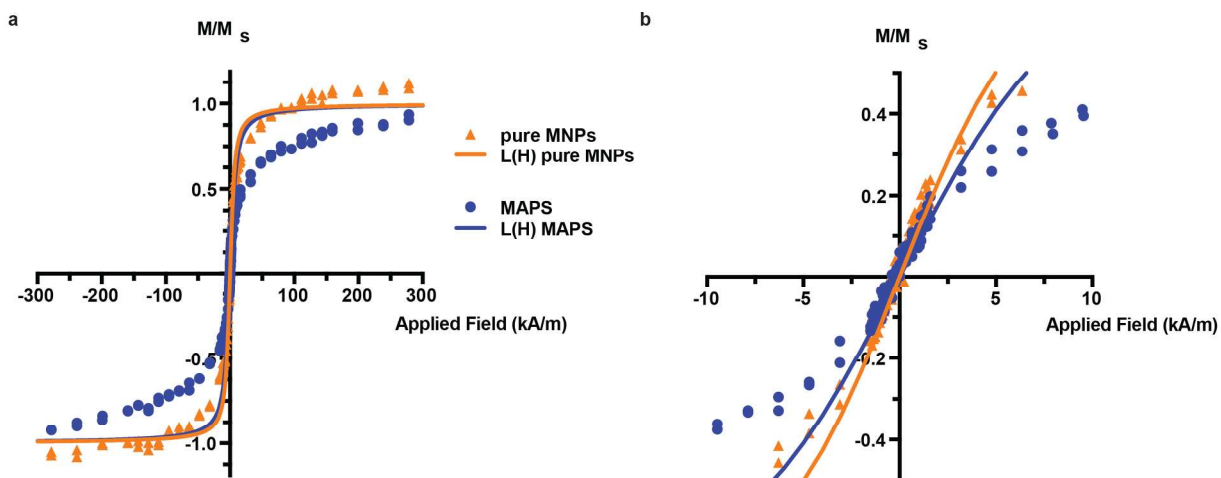
Figure S3. Characterization of sample magnetization. **(a)** Vibrating sample magnetometry data with Langevin fit L(H) are shown for MAPS and free MNPs solutions in PBS for applied fields ranging from -300 to +300 kA/m. In **(b)** an expanded view of the data in **(a)** in the vicinity of zero applied field is presented highlighting that both, the encapsulated and free magnetic nanoparticles, converge to nearly the same slope in the limit of low applied fields. However, the encapsulated MNPs approach saturation more gradually than the free particles as evident in (a). Both of these qualitative features are predicted for noninteracting ensembles of randomly oriented particles with increasing anisotropy. Increased concentration has been shown to slow reversal, raise the blocking temperature, and give rise to hysteresis at low temperatures in densely concentrated samples. Since liposomes provide an environment with locally enhanced particle concentration, it is plausible this could give rise to effects analogous to increased anisotropy that, while maintaining superparamagnetic behavior at the timescale of seconds, could play a role in heat dissipation at high frequencies.
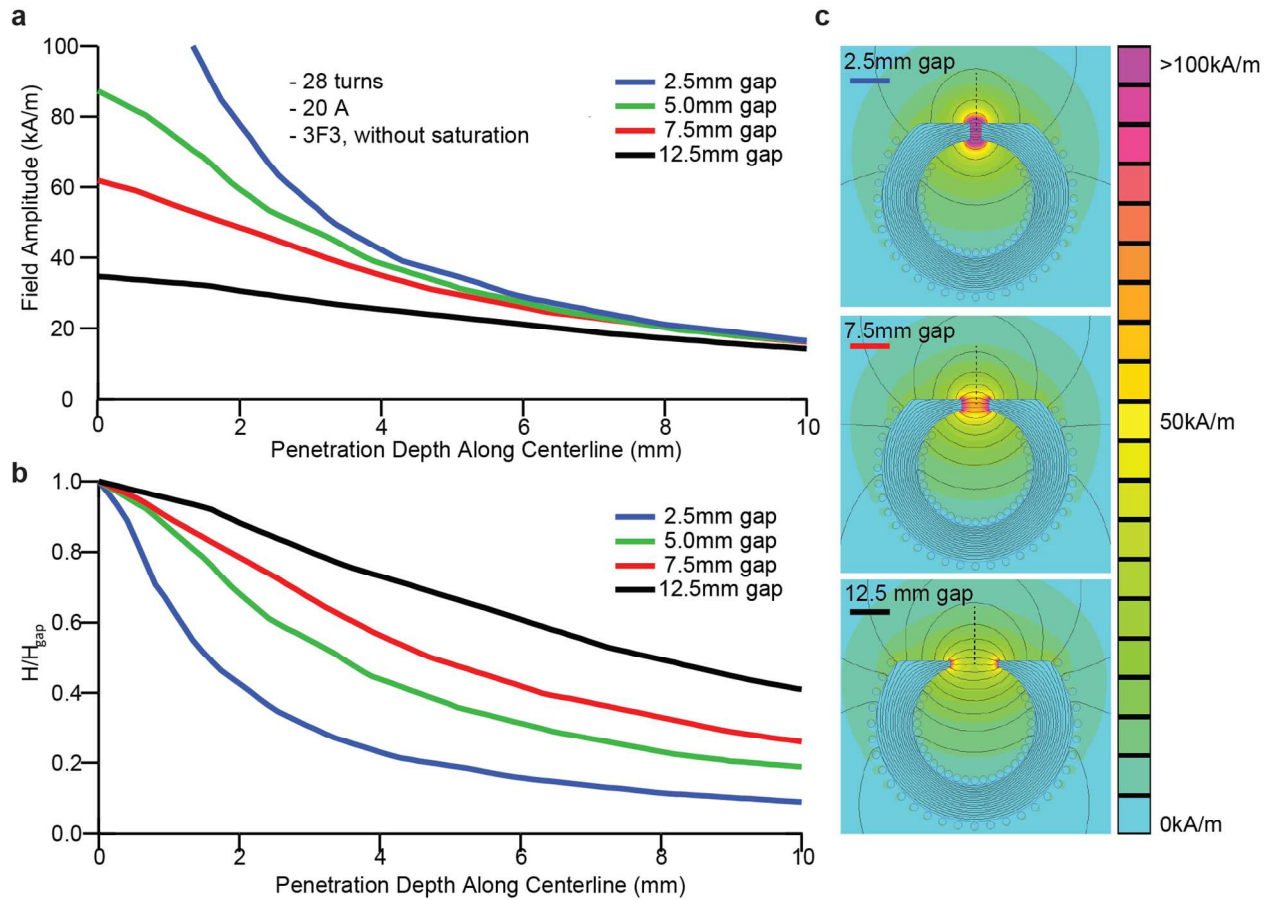
Figure S4. Simulations of field amplitude for varying gap sizes. Coils are simulated with 28 turns of litz wire and ferromagnetic core material (3F3) at 20 A input current. The decay of the field amplitude along the center line (black dotted line in (c)) is plotted for gap sizes ranging from 2.5-12.5 mm size **(a)** as well as the relative decay with distance with respect to the field strength achieved at the center of the gap **(b)**. The spatial distribution of the field strength across these different gap designs is depicted in **(c)**.
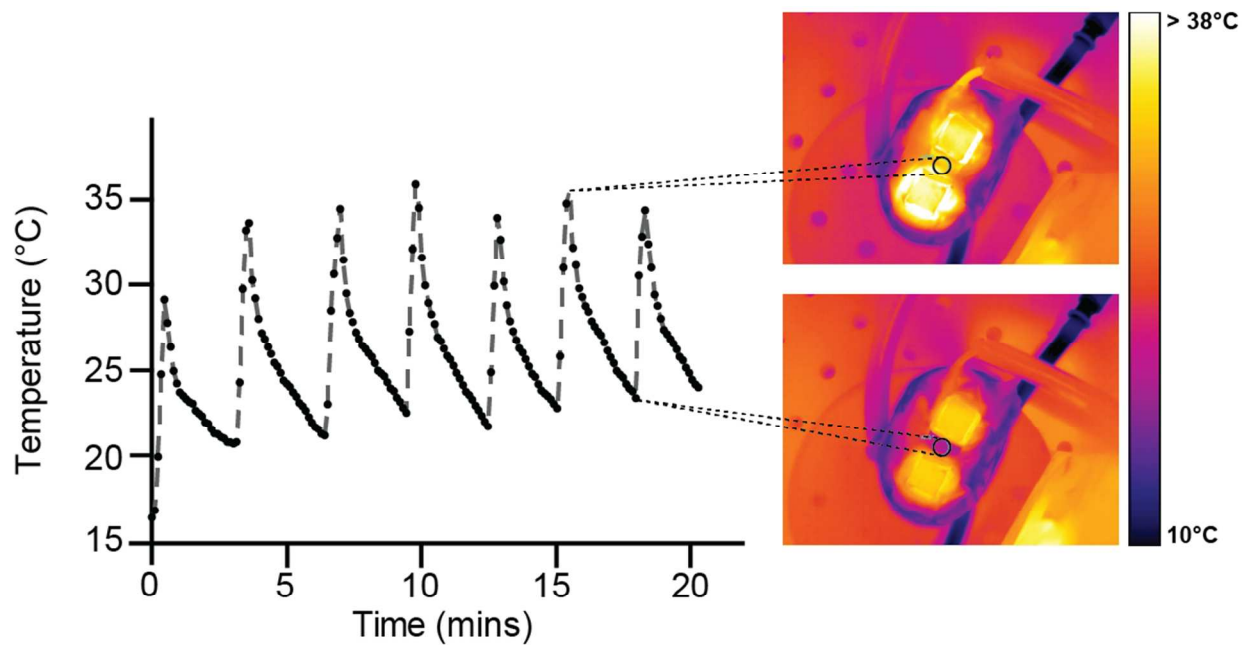
Figure S5. IR measurements during operation. The temperature profile of the coil was measured during a number of duty cycles by using an infrared camera (FLIR TC 650sc). A circular area of 10 mm diameter in the center of the coil gap was determined, covering the area tumors were exposed to (see right). The average temperature values recorded in that area are plotted over time (left, also shown in Fig. 3c in main text), not exceeding 36°C.

Table S1. Sequences of peptides employed in study.

Peptide Name	Sequence
S1	Biotin-CGPVGLIGK(Cy7)eGvndneeGffsar-NH$_2$
S2	Biotin-CGPVPLSLVMK(Cy7)eGvndneeGffsar-NH$_2$
S3	Biotin-CGPLGVRGKK(Cy7)eGvndneeGffsar-NH$_2$

Legend

Fluorophore   Protease substrate   For isolation of uncleaved substrates

Molecular spacers   Urinary reporter

lower case = D stereoisomer

a Uncleaved Peptide Purification Method

b PBS
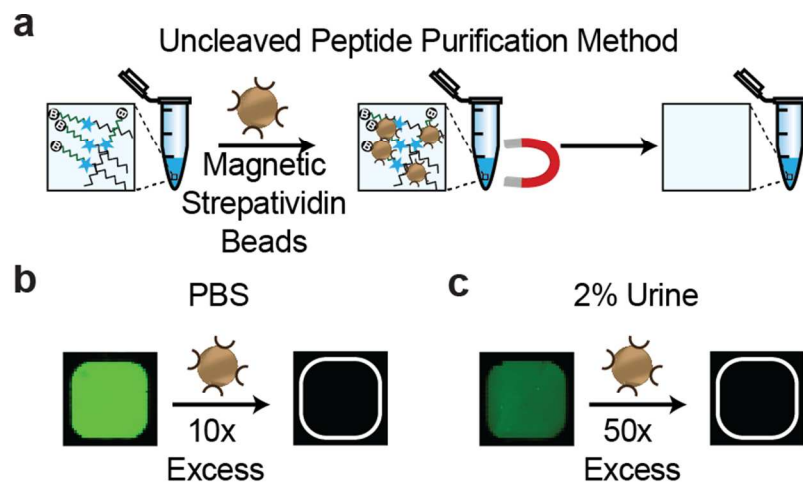
c 2% Urine

Figure S6. Urine depletion of uncleaved substrates. (**a**) Approach for isolating uncleaved substrate-reporter tandems. (**b**) Demonstration of depletion in PBS and (**c**) 2% urine.
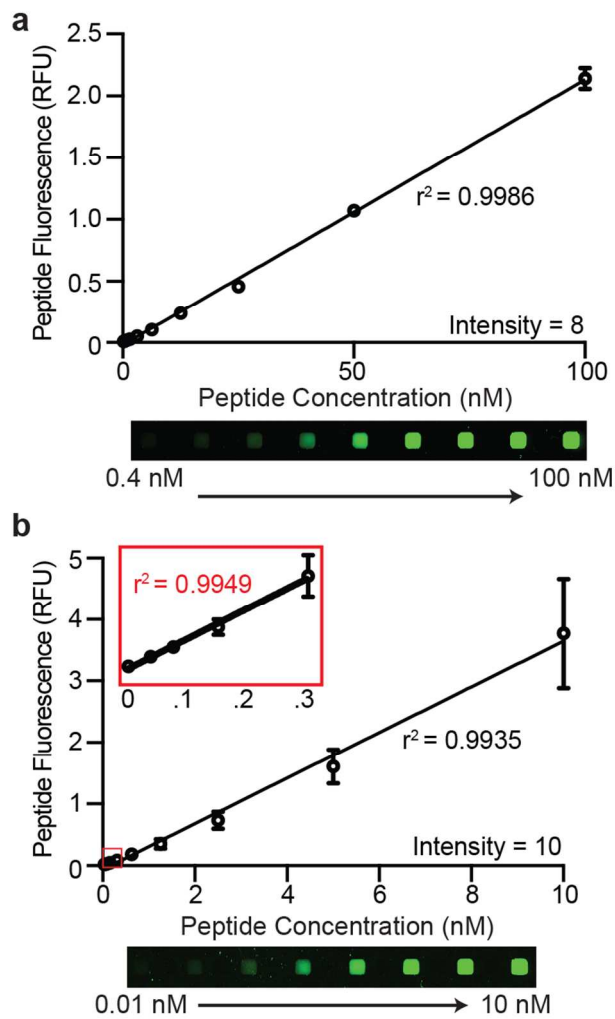
Figure S7. Cy7 ladder reading on IR scanner. Scanner is sensitive to large dynamic range of peptide concentrations at different intensity gains (**a**) enabling both high and (**b**) low peptide concentration quantification.
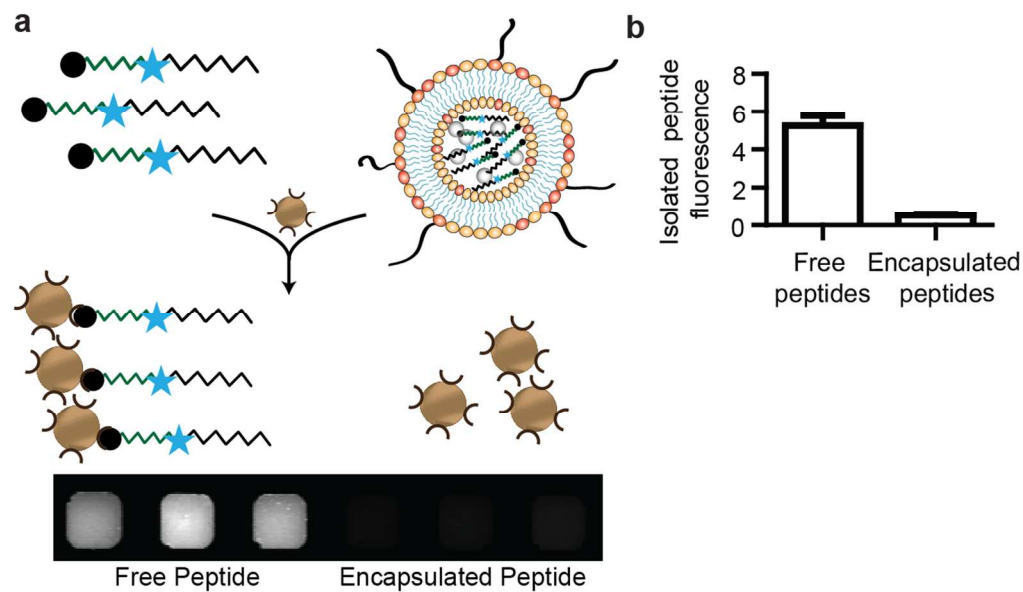
Figure S8. Peptides are shielded inside liposomes. (**a**) We queried if streptavidin beads could bind to unencapsulated peptides inside liposomes after synthesis and purification. When peptide was encapsulated very little fluorescence was detected. (**b**) Quantification of peptide fluorescence isolated by streptavidin beads.
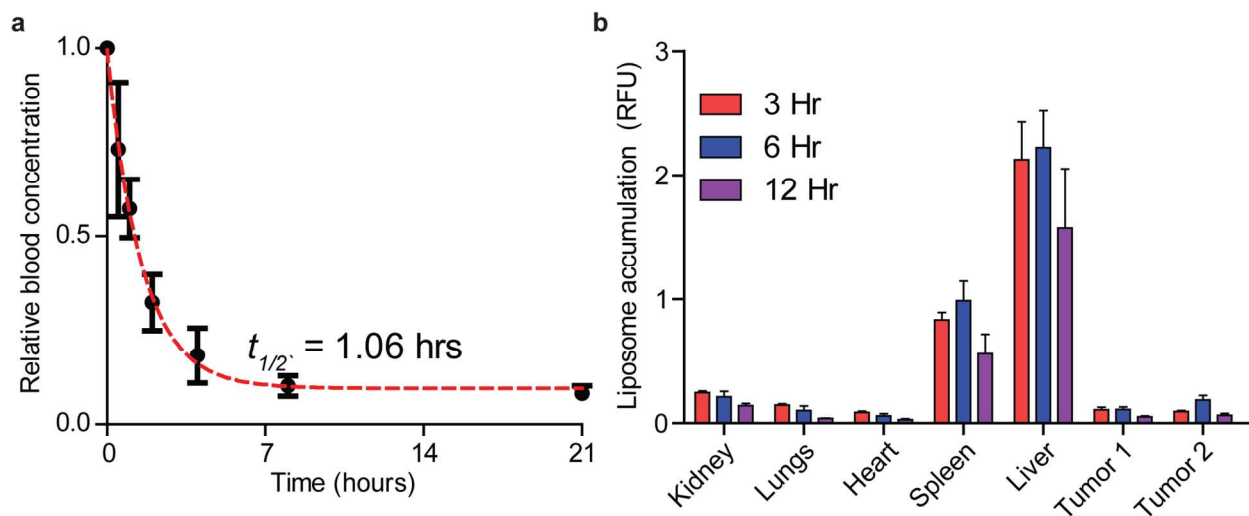
Figure S9. Pharmacokinetic characterization of MAPS. (**a**) Plasma concentration of fluorescently labeled liposomes was fit to a one-phase exponential decay equation. (**b**) Organs and tumors were harvested after 3, 6 and 12 hours and accumulation of MAPS was measured by an IR scanner.
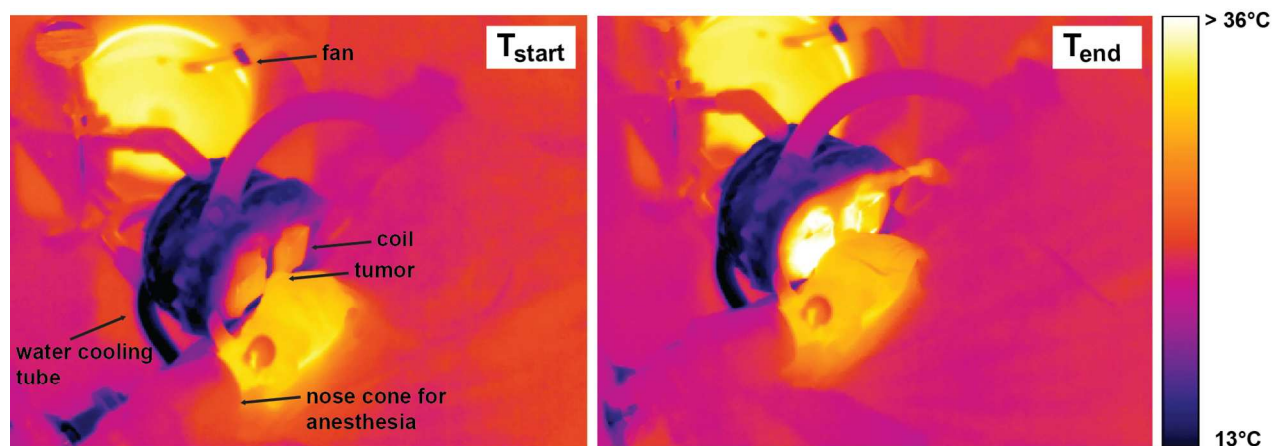
Figure S10. IR measurements during *in vivo* operation. No specific heating of the animals at the location of the coil could be observed using thermal camera recordings at the beginning, T_{start} = 0 s, and end, T_{end} = 320 sec, of an *in vivo* duty cycle consisting of 40 sec AMF exposures separated by 240 sec rest.
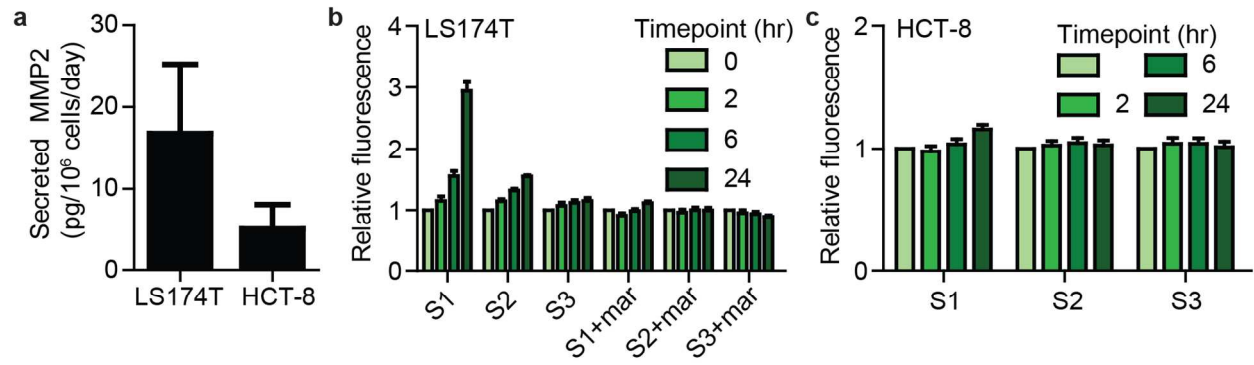
Figure S11. *In vitro* cellular protease analysis and comparison. (**a**) Secreted MMP2 levels between LS174T and HCT-8 as measured by an ELISA. (**b**) Proteolysis of quenched substrates 1-3 over time by conditioned media from LS174T cells. Mar = marimastat, an MMP inhibitor. (**c**) Cleavage of S1-3 by secreted proteases from conditioned media from HCT-8 cells.
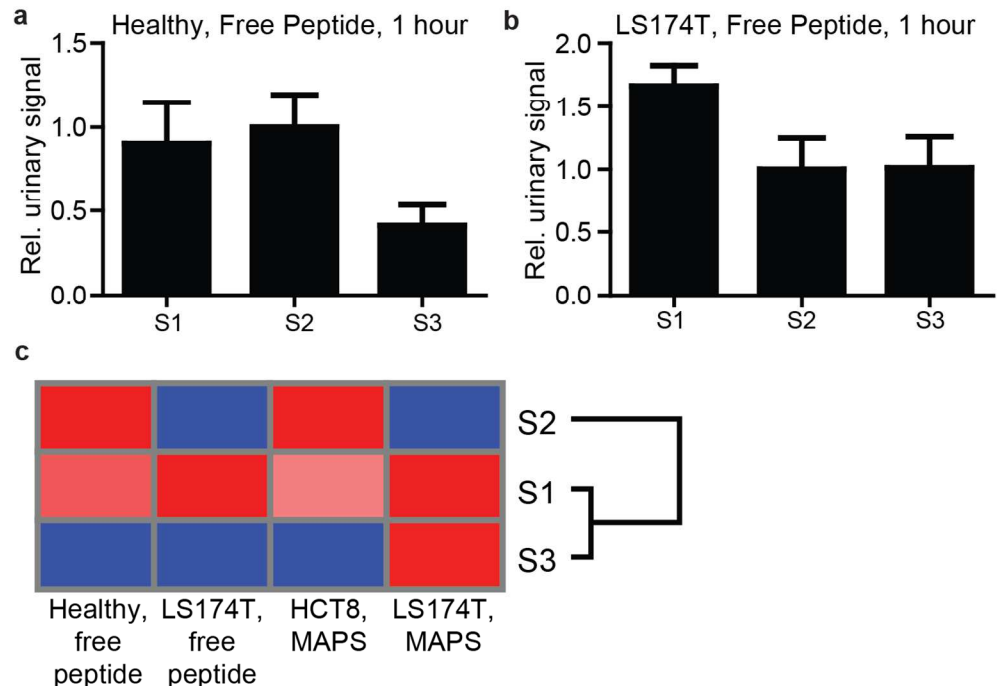
Figure S12. *In vivo* **performance of unencapsulated S1-3 peptides.** (**a**) Free peptides injected into healthy nude mice showed S3 with lowest background proteolysis. (**b**) Free peptides injected into LS174T flank tumor bearing mice show different proteolysis pattern than MAPS (all data normalized to S2 urine signal). (c) Heatmap and clustering of all *in vivo* experiments reflects similar performance of S1 and S3 as seen in the *in vitro* experiments.